PCCP

Cite this: *Phys. Chem. Chem. Phys.*, 2012, **14**, 11651–11656

www.rsc.org/pccp

PAPER

Vibrational energy relaxation of the ND-stretching vibration of NH_2D in liquid NH_3

Tim Schäfer,[a] Alexander Kandratsenka,*[ab] Peter Vöhringer,[c] Jörg Schroeder[a] and Dirk Schwarzer[b]

Received 30th April 2012, Accepted 3rd July 2012
DOI: 10.1039/c2cp41382e

The vibrational energy relaxation from the first excited ND-stretching mode of NH_2D dissolved in liquid NH_3 is studied using molecular dynamics simulations. The rate constants for inter- and intramolecular energy transfer are calculated in the framework of the quantum-classical Landau–Teller theory. At 273 K and an ammonia density of 0.642 g cm^{-3} the calculated ND-stretch lifetime of $\tau = 9.1$ ps is in good agreement with the experimental value of 8.6 ps. The main relaxation channel accounting for 52% of the energy transfer involves an intramolecular transition to the first excited state of the umbrella mode. The energy difference between both states is taken up by the near-resonant bending vibrations of the solvent. Less important for the ND-stretch lifetime are both the direct transition to the ground state and intramolecular relaxation *via* the NH_2D bending modes contributing 23% each. Our calculations imply that the experimentally observed weak density dependence of τ is caused by detuning the resonance between the ND-stretch–umbrella energy gap and the solvent accepting modes which counteracts the expected linear increase of the relaxation rate with density.

1 Introduction

Studies of vibrational energy relaxation (VER) in the liquid phase can help to gain a better understanding of dynamic interactions of solutes with surrounding bath molecules.[1–3] Since these interactions play a central role in chemical reactions in the condensed phase, it is of great significance to analyze such processes in detail and quantify the contributions of different relaxation pathways. Numerous studies of this kind have focused on aqueous systems,[4–20] recently, they have been expanded to condensed ammonia.[21] Like water, liquid ammonia is a well studied ionizing solvent. Due to its potential to dissolve alkali metals and to form solvated electrons, such solutions are used in organic chemistry as reducing agents (*e.g.*, Birch reaction).[22–24]

Although liquid ammonia is often cited in chemistry textbooks as an example for associated liquids forming extended hydrogen bond networks,[25] neutron scattering experiments[26,27] and computer simulations based on Car–Parinello *ab initio* molecular dynamics[28] (MD) and mixed quantum/classical molecular dynamics[29] show that, in contrast to water, hydrogen bonding is of negligible importance. Consequently, the characteristics of the dynamics of VER in ammonia over a wide thermodynamical range differ from the well studied behavior of water. This was recently demonstrated by pump–probe absorption spectroscopy experiments, where the ND-stretching fundamental of NH_2D in NH_3 was excited by a femtosecond pulse and the lifetime of the stretching mode was observed over a wide range of temperature and pressure (230–450 K, 10–1500 bar).[21] At 273 K and a solvent density of 0.642 g cm^{-3} the lifetime of the excited ND-stretch vibration of NH_2D was measured to be 8.6 ps which is much larger than typical vibrational lifetimes of liquid water at comparable conditions (about 1 ps).[11,12]

These experimental studies were supported by simple theoretical calculations of the ND-stretch lifetime[21] based on the Landau–Teller (LT) approach. Here a breathing-sphere model described the solute molecule, and solvent molecules were modeled as point masses. This model describes the temperature dependence but it cannot distinguish between different relaxation pathways, since it does not take into account rotations and intramolecular vibrations of the solvent. It is therefore desirable to use the more sophisticated approach already applied successfully to the water system such as advanced LT theory[30–34] and non-equilibrium molecular dynamics simulations.[35–40]

In this work we use the Landau–Teller approach following the lines developed by Rey and Hynes[31] and Lawrence and Skinner[33] in order to study in detail the vibrational energy relaxation pathways from the excited N–D stretching mode of

[a] *Institut für Physikalische Chemie, Universität Göttingen, Tammannstrasse 6, 37077 Göttingen, Germany. E-mail: akandra@gwdg.de; Fax: +49 551 201 1501; Tel: +49 551 201 2004*
[b] *Max-Planck-Institut für Biophysikalische Chemie, Am Faßberg 11, 37077 Göttingen, Germany*
[c] *Abteilung für Molekulare Physikalische Chemie, Institut für Physikalische und Theoretische Chemie, Rheinische Friedrich-Wilhelms-Universität, Wegelerstraße 12, 53115 Bonn, Germany*

NH_2D in a NH_3 solution. The results of the LT calculations are then compared to the experimental measurements.[21]

2 Theoretical background

2.1 Landau–Teller approach

In the LT approach Fermi's Golden Rule is used to calculate the vibrational transition rates which are expressed in terms of the time correlation function (TCF) of the system–bath interaction potential.[30] The full quantum-mechanical calculation of a TCF is not feasible, therefore the part of the TCF related to the bath degrees of freedom is calculated classically from equilibrium molecular dynamics (MD) simulations and quantum effects are taken into account by using a quantum correction factor (QCF).

The Hamiltonian of a solute NH_2D in the bath of NH_3 molecules can be written in the form

$$H = H_S + H_B + V, \quad (1)$$

where H_S is the vibrational Hamiltonian of NH_2D, H_B describes the bath including the rotational and translational degrees of freedom of the solute, and V stands for the coupling between the molecular vibrational coordinates of the solute NH_2D and the surrounding bath molecules. Coriolis and centrifugal couplings are assumed to play a minor role in the VER processes,[31] and consequently will be neglected. The system–bath coupling operator V is expanded to first order in the six NH_2D dimensionless normal coordinates $\{q_s\}$:

$$V = -\sum_s q_s F_s, \quad F_s = -\left.\frac{\partial V}{\partial q_s}\right|_{q_s=0}. \quad (2)$$

Hence the rate constant k_{ij} for a transition from the initial vibrational state i to the final state j is given by the expression

$$k_{ij} = Q(\omega_{ij}) \int_{-\infty}^{\infty} \mathrm{d}t\, \mathrm{e}^{i\omega_{ij}t} \sum_{s,s'} \langle i|q_s|j\rangle\langle j|q_{s'}|i\rangle\langle F_s F_{s'}(t)\rangle, \quad (3)$$

where $\langle F_s F_{s'}(t)\rangle$ is the classical TCF of the normal forces corresponding to the s and s' normal coordinates, and $Q(\omega_{ij})$ is the quantum correction factor depending on the vibrational Bohr frequency ω_{ij}. The matrix elements $\langle i|q_s|j\rangle$ for the NH_2D vibrational degrees of freedom are calculated quantum-mechanically from the anharmonic eigenfuntions $|i\rangle$.

2.2 Matrix elements calculation

For the NH_2D molecule we use the intramolecular potential by Martin *et al.*[41]

$$U_{NH_2D} = \frac{1}{2}\sum_{i,j} f_{ij}\xi_i\xi_j + \Lambda, \quad (4)$$

$$\Lambda = \frac{1}{6}\sum_{i,j,k} f_{ijk}\xi_i\xi_j\xi_k + \frac{1}{24}\sum_{i,j,k,\ell} f_{ijk\ell}\xi_i\xi_j\xi_k\xi_\ell, \quad (5)$$

where the internal coordinates

$$\xi_i = \{\Delta r_{NH_1}, \Delta r_{NH_2}, \Delta r_{ND}, \Delta\phi_{H_1NH_2}, \Delta\phi_{H_1ND}, \Delta\phi_{H_2ND}\}$$

describe the deviations from the equilibrium bond length of 1.0141 Å and from the equilibrium valence angle of 105.64°.

Table 1 Vibrational frequencies (in cm^{-1}) of NH_2D for the potential U_{NH_2D} from eqn (4) and experimental data

Vibration	Harmonic	Fundamental	Measured[42]
ν_{3b} (asym. NH-stretch)	3597	3416	3439
ν_{3a} (sym. NH-stretch)	3517	3350	3366
ν_1 (ND-stretch)	2587	2491	2506
ν_{4a} (sym. bending)	1654	1604	1598
ν_{4b} (asym. bending)	1440	1403	1390
ν_2 (umbrella)	1022	962	886

The term Λ contains the anharmonic contributions to the intramolecular potential. The calculated frequencies for the potential (4) together with their experimental values are listed in Table 1 showing sufficient accuracy for our purposes. The importance of anharmonicity is also demonstrated by comparison with harmonic frequencies.

Standard methods[43] were used to perform the normal mode analysis of the solute molecule and to express the intramolecular potential energy U_{NH_2D} in terms of the normal mode coordinates q_s up to fourth order.

To calculate the matrix elements of q_s the first-order perturbation theory expression[44]

$$\langle i|q_s|j\rangle = \langle i_0|q_s|j_0\rangle + \sum_{k\neq i,j} \frac{\Lambda_{ik}\langle k_0|q_s|j_0\rangle}{E_i^{(0)} - E_k^{(0)}} + \sum_{k\neq j,i} \frac{\Lambda_{kj}\langle i_0|q_s|k_0\rangle}{E_j^{(0)} - E_k^{(0)}}, \quad (6)$$

was utilized where Λ_{ik} are matrix elements of the anharmonic potential energy operator (5) and the index '0' refers to the six-dimensional harmonic eigenfunction of the NH_2D (ordered according to their vibrational frequency):

$$|i_0\rangle = |n_{3b}n_{3a}n_1n_{4a}n_{4b}n_2\rangle \quad (7)$$

with n_i denoting the quantum number of the ith mode.

Table 2 shows the values of the matrix elements for transitions that contribute to the main VER pathways (see discussion in Section 3.1). As expected, the matrix elements that do not vanish in the harmonic approximation have the largest values due to contributions from the undisturbed matrix elements $\langle i_0|q_s|j_0\rangle$. Those matrix elements correspond to direct transitions from the excited ND-stretch, symmetric and asymmetric bend, and umbrella mode to the ground state ($\langle 001000|q_1|000000\rangle$,

Table 2 Largest values for the squared matrix elements defined by eqn (6) for transitions that contribute to the main VER pathways. The states are denoted following eqn (7)

$\langle 001000\|q_1\|000000\rangle^2$	0.488
$\langle 001000\|q_2\|000100\rangle^2$	1.96×10^{-3}
$\langle 001000\|q_1\|000001\rangle^2$	1.94×10^{-3}
$\langle 001000\|q_{4b}\|000010\rangle^2$	1.75×10^{-3}
$\langle 001000\|q_{4b}\|000002\rangle^2$	1.7×10^{-4}
$\langle 001000\|q_2\|000101\rangle^2$	8.3×10^{-6}
$\langle 001000\|q_{4b}\|000011\rangle^2$	3.5×10^{-6}
$\langle 001000\|q_{4b}\|000110\rangle^2$	9.9×10^{-7}
$\langle 000100\|q_{4a}\|000000\rangle^2$	0.521
$\langle 000100\|q_2\|000001\rangle^2$	7.09×10^{-3}
$\langle 000100\|q_{4b}\|000010\rangle^2$	1.27×10^{-3}
$\langle 000010\|q_{4b}\|000000\rangle^2$	0.520
$\langle 000010\|q_{3b}\|000001\rangle^2$	7.38×10^{-4}
$\langle 000001\|q_2\|000000\rangle^2$	0.541

$\langle 000100|q_{4a}|000000\rangle$, $\langle 000010|q_{4b}|000000\rangle$ and $\langle 000001|q_2|000000\rangle$, respectively).

It should be noted that small values of the other matrix elements do not imply that the corresponding contribution to the total rate coefficient are negligible, because each contribution is given by a product of the matrix element and the spectral density of external forces at the frequency of the energy gap ω_{ij} (see eqn (3)).

2.3 Force power spectrum

In the framework of the LT approach the force power spectrum

$$S_{ss'}(\omega_{ij}) = \int_{-\infty}^{\infty} \mathrm{d}t\, \mathrm{e}^{i\omega_{ij}t}\langle F_s F_{s'}(t)\rangle \tag{8}$$

is calculated from classical equilibrium MD simulations.

We performed those calculations for a system consisting of a rigid NH_2D molecule in its equilibrium geometry[41] and 100 flexible NH_3 molecules in a cubic box with periodic boundary conditions. The solvent intramolecular force field[45]

$$\begin{aligned} U_{NH_3} &= \frac{\kappa_s}{2}(\Delta r^2_{NH_1} + \Delta r^2_{NH_2} + \Delta r^2_{NH_3}) \\ &+ \frac{\kappa_b}{2}(\Delta\phi^2_{H_1NH_2} + \Delta\phi^2_{H_1NH_3} + \Delta\phi^2_{H_2NH_3}) \end{aligned} \tag{9}$$

was used with force constants κ_s = 3824.0 kJ (mol Å^2)$^{-1}$ and κ_b = 333.3 kJ mole^{-1} and the equilibrium valence bond length $r^{(eq)}_{NH}$ = 1.024 Å and valence angle $\phi^{(eq)}_{HNH}$ = 111.79°. The intermolecular interactions were modeled with a Lennard-Jones potential applied only to the nitrogen atoms with parameters ε = 5.654 kJ mole^{-1}, σ = 3.385 Å and a Coulomb potential with partial charges q_H = 0.345 e and q_N = −1.035 e.[46]

The simulations were performed using the modified Beeman algorithm[47] with Ewald summation handling the electrostatic forces.[48] Density and temperature were chosen to match the experimental conditions (0.642 g cm^{-3} and 273 K). After scaling the kinetic energy (100 ps) to the desired temperature and equilibration of the system (50 ps) a long run of 1 ns in timesteps of 0.1 fs was performed. Positions of the NH_2D atoms and the forces acting on them were saved in time intervals of 4 fs.

The projections of forces on the NH_2D vibrational normal modes were calculated by means of the equation

$$F_s(t) = \sum_a F_a(t)\cdot\hat{R}(t)\cdot\ell_{s,a}, \tag{10}$$

where $\hat{R}$ is the rotation matrix from the laboratory frame to the molecular body-fixed frame and $\ell_{s,a}$ is the sth normal mode displacement vector for an atom a defined for the NH_2D static configuration. Finally, standard methods were used to calculate the TCF and its Fourier transform.[49]

We used the Harmonic–Schofield QCF ($\beta = (k_B T)^{-1}$)

$$Q(\omega) = \sqrt{\frac{\beta\hbar\omega}{1-\mathrm{e}^{\beta\hbar\omega}}\mathrm{e}^{\beta\hbar\omega/2}} \tag{11}$$

which was shown to be an adequate choice in different studies.[33,34,50]

3 Results and discussion

3.1 Vibrational energy relaxation pathways

The ammonia molecule has six fundamental vibrations, where due to its high symmetry (C_{3v}) the asymmetric stretching and asymmetric bending modes are both twofold degenerate. Monodeuteration of the ammonia molecule leads to a decrease of its symmetry and, hence, to a lifting of vibrational degeneracies. The vibrational frequencies of the solute NH_2D and the solvent NH_3 are shown for the gas phase as well as for the liquid phase in Table 3.

All stretching vibrational frequencies of the liquid phase are red-shifted relative to their gas phase values, while the absorption bands of the bending modes show a blue shift. These tendencies are similar to water, but less pronounced.[11,12]

Considering the possible relaxation pathways from the initially excited ND-stretching mode (ν_1), it is obvious that the NH-stretching vibrations (ν_{3a} and ν_{3b}) of NH_2D play a minor role, because their fundamental excitations are too high in energy relative to the initially prepared ND-stretching fundamental (Table 3). However, the first excited states of all the other vibrations are below the ND-stretching fundamental and can therefore be transiently populated during the course of VER.

Fig. 1 shows the power spectra of external forces acting on the six normal modes of NH_2D calculated from the MD simulations. They all are very similar in shape and characterized by a strong decay with increasing frequency to which resonance

Table 3 Experimental vibrational frequencies (in cm^{-1}) of NH_2D and NH_3 in the liquid and in the gas phase. The degeneracy of ν_3 and ν_4 in NH_3 is lifted in NH_2D

	NH_2D		NH_3	
Vibration	Gas[42]	Liquid[21]	Gas[51]	Liquid[52]
ν_1	2506	2445	3336	3300
ν_2	886		933	1060
ν_{3a}	3366		3443	3381
ν_{3b}	3439			
ν_{4a}	1598		1626	1630
ν_{4b}	1390			

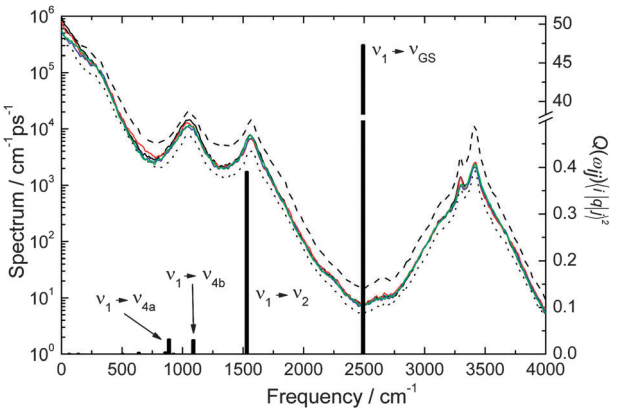

Fig. 1 Power spectra of forces acting on the six normal modes of NH_2D ν_1, ν_{3b}, ν_{4a}, ν_{4b} (solid), ν_2 (dashed), ν_{3a} (dotted) in NH_3 at 273 K, 0.642 g cm^{-3}.

peaks of the solvent NH_3 umbrella (about 1000 cm^{-1}), bending (about 1600 cm^{-1}), and stretching (about 3300 cm^{-1}) vibrations are superimposed. As the relaxation rate is given by the product of the force power spectrum and the squared matrix element (eqn (3)), values of the latter multiplied by the QCF are shown for the main transitions from the excited ND-stretch mode in Fig. 1 as well (black bars, right ordinate). Compared to the force power spectra the bars show an opposite trend: their amplitudes increase with frequency. As a result the most efficient relaxation transition appears at an intermediate frequency, *i.e.* from the ND-stretch to the first excited state of the umbrella mode of NH_2D, $\nu_1 = 1 \rightarrow \nu_2 = 1$, with a time constant of 17.4 ps. The energy difference of 1530 cm^{-1} is transferred to the almost resonant bending vibrations of the NH_3 solvent.

The relaxation times for all transitions depopulating the ND-stretch $\nu_1 = 1$ state are summarized in the upper part of Table 4. The direct transition from the first excited ND-stretch state to the ground state, $\nu_1(1 \rightarrow 0)$, has the largest matrix element, however, at that energy gap of 2491 cm^{-1} the amplitude of the corresponding force spectrum is very low. In other words, the NH_3 bath can hardly provide an energy accepting mode at that particular frequency. Consequently, the relaxation time for that pathway is 40.1 ps. On the other hand, for the intramolecular transitions to the excited bending states ν_{4a} and ν_{4b} (82.6 ps and 74.5 ps, respectively) or even to the almost isoenergetic $\nu_2 + \nu_{4a}$ combination mode (877 ps) the corresponding amplitude of the force power spectrum is relatively high. But at the same time the matrix elements are so small that these pathways become unimportant. From the relaxation times for the individual channels the vibrational lifetime of the $\nu_1 = 1$ state can be calculated. We obtain $\tau = 9.1$ ps which is in excellent agreement with the experimentally observed value of 8.6 ps.[21]

In the lower part of Table 4 the relaxation times of the excited bending modes ν_{4a} and ν_{4b} and the umbrella mode ν_2 are listed. All three vibrations have sub-picosecond lifetimes and are dominated by direct one quantum transitions to the ground state. The umbrella vibration is the lowest frequency mode in the NH_2D molecule. Furthermore, it is in close resonance to the umbrella vibration of the NH_3 solvent which opens an effective relaxation pathway with a time constant of $\tau = 150$ fs. In principle, for the bending modes also intramolecular relaxation channels are available. However, their matrix elements are so small that they can be neglected. The frequency of the symmetric bending mode ν_{4a} is closer in resonance with the degenerate ν_4 vibration of NH_3 than the asymmetric bend ν_{4b}. Thus the lifetime of ν_{4a} is substantially shorter ($\tau = 140$ fs) than the one of ν_{4b} ($\tau = 570$ fs). Since all vibrational states of NH_2D located below the $\nu_1 = 1$ state have subpicosecond lifetimes the depopulation of the initially excited ND-stretch vibration determines the rate of the whole relaxation process and no population can be accumulated in the lower vibrational states.

In Fig. 2 the pathways depopulating the excited $\nu_1 = 1$ state are shown graphically using arrows whose thicknesses are proportional to their contribution. The main relaxation channel responsible for 52% of the energy dissipation is the transition *via* the first excited state of the umbrella mode to the ground state whereas the direct transition to the ground state contributes with 23%. The pathways *via* the bending modes ν_{4a} and ν_{4b} carry a relative weight of 11% and 12%, respectively.

It is worth mentioning that the choice of the QCF has a strong impact on the calculated vibrational energy relaxation lifetimes and pathways. In particular for high frequency modes the QCFs differ considerably. Consequently, the ND-stretch vibrational lifetimes presented in Table 5 are mainly influenced by various contributions of the direct transition to the ground state $|001000\rangle \rightarrow |000000\rangle$. The choice of using the Harmonic–Schofield QCF mainly rests on the observation that both the Harmonic and the Standard factor distinctly underestimate measured relaxation rates.[53,54] This is consistent with our

Table 4 Transition frequencies and relaxation times from excited NH_2D vibrational states

Transition	ω_{ij}/cm^{-1}	τ/ps
Relaxation from ND-stretch		
$\|001000\rangle \rightarrow$		
$\|000001\rangle$	1530	17.4
$\|000000\rangle$	2491	40.1
$\|000010\rangle$	1089	74.5
$\|000100\rangle$	888	82.6
$\|000101\rangle$	−64	877
$\|000002\rangle$	639	1205
$\|000011\rangle$	139	7000
$\|000110\rangle$	−506	202 000
Total		9.1
Relaxation from symmetric bend		
$\|000100\rangle \rightarrow$		
$\|000000\rangle$	1604	0.14
$\|000001\rangle$	642	17.9
$\|000010\rangle$	201	34.3
Total		0.14
Relaxation from asymmetric bend		
$\|000010\rangle \rightarrow$		
$\|000000\rangle$	1403	0.57
$\|000001\rangle$	441	323.7
Total		0.57
Relaxation from umbrella		
$\|000001\rangle \rightarrow$		
$\|000000\rangle$	962	0.15

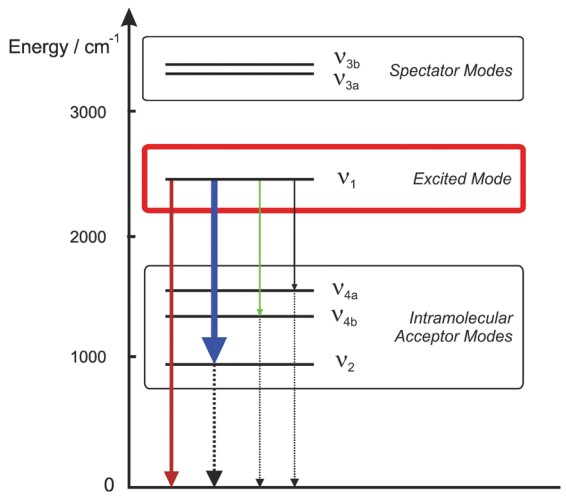

Fig. 2 Vibrational energy relaxation pathways for the excited ND-stretching vibration. The thickness of the arrow represents the contribution of a given transition calculated from the last column of Table 4.

Table 5 ND-stretch vibrational lifetimes calculated with different QCF

Quantum correction factor	τ_r/ps
Standard $\left(\frac{2}{1+e^{-\beta\hbar\omega}}\right)$	76.8
Harmonic $\left(\frac{\beta\hbar\omega}{1-e^{-\beta\hbar\omega}}\right)$	24.4
Harmonic–Schofield (eqn (11))	9.1
Schofield ($e^{\beta\hbar\omega/2}$)	2.8

studies justifying the choice of the Harmonic–Schofield QCF factor.

3.2 Density dependence of VER

The experimental data on the VER of the ND-stretch vibration of NH_2D in supercritical NH_3 showed an amazingly weak dependence of relaxation rate on the solvent density,[21] *e.g.* at 452 K the relaxation rate constant increased by only 30% when the NH_3 density was doubled. It was suggested that this effect is caused by detuning effects, *i.e.* energetic shifts of the vibrational states responsible for vibration to vibration (V–V) energy transfer. Our calculations allow for testing this conjecture in more detail.

Table 3 shows a comparison of the experimental vibrational frequencies of NH_2D and NH_3 for the gas and liquid phase, respectively. At first, we analyze the shift of the energy gap for the most important relaxation channel $\nu_1 = 1 \rightarrow \nu_2 = 1$ in the NH_2D molecule. Upon passing from the gas to the liquid phase the ND-stretch mode shifts to lower frequencies whereas the umbrella mode shows the opposite trend (the latter has not been measured directly for the NH_2D molecule but for NH_3). This implies that the ND stretch-to-umbrella energy gap decreases when the solvent density is increased. At the same time the frequency of the energy accepting (degenerate) bending modes ν_4 of NH_3 is almost density independent. The consequences of these effects are presented in Fig. 3 where the power spectrum of normal forces acting on the umbrella mode of NH_2D at the frequency of the $\nu_1 = 1 \rightarrow \nu_2 = 1$ transition is shown. One can see that the transition energy appears at the low frequency edge of the resonance peak generated by the ν_4 bending vibration of NH_3. When the density increases the power spectral density will increase as well with no shift of the peak position since the frequency of the ν_4 mode is almost density independent. However, at the same time the energy gap of the $\nu_1 = 1 \rightarrow \nu_2 = 1$ transition will shift to lower frequency such that the acceleration of the relaxation rate is less than expected from the pure density change of the solvent.

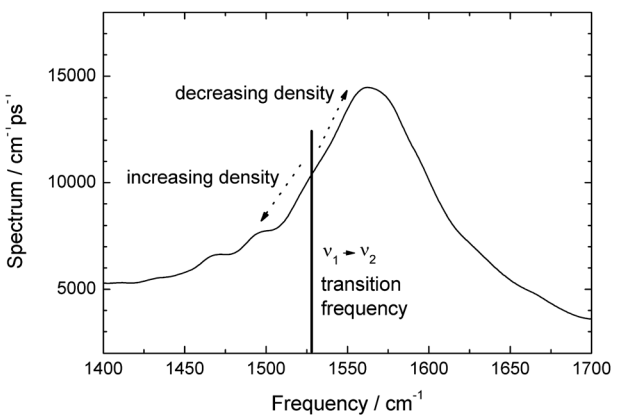

Fig. 3 The ν_2 normal force power spectrum of NH_2D in NH_3 at the spectral region of the $\nu_1 = 1 \rightarrow \nu_2 = 1$ energy gap. With decreasing density the transition frequency approaches the maximum of the bending mode.

4 Conclusion

We examined the lifetime of the ND-stretching vibration of NH_2D in NH_3 using a Landau–Teller approach along the lines developed by Rey and Hynes[31] and Lawrence and Skinner.[33] The computed value of 9.1 ps is in excellent agreement with the experimental value of 8.6 ps. The main ND-stretch relaxation pathways are the transition to the umbrella mode (52%) and the direct transition to the ground state (23%). In the preceding experimental work[21] a weak density dependence of the ND-stretch lifetime was observed. The results of this theoretical study strongly suggest that with decreasing solvent density the intermolecular acceptor modes become increasingly resonant with the ND-stretching to umbrella transition. This leads to a more effective vibrational energy transfer that causes a shorter lifetime at low densities than expected from the stretched exponential decay of the force power spectrum.

The analysis of the density dependence of the rate constant is qualitative and schematic, since gas phase potentials were used to calculate the matrix elements of normal coordinates listed in Table 2. MD simulations with more realistic potentials therefore would be desirable for a more complete insight into the ammonia vibrational relaxation process. Further the choice of the adequate QCF is still a challenge in this kind of calculations.[53,54] We chose the Harmonic–Schofield QCF, since it was successfully used for similar systems.[33,34,50]

Acknowledgements

Financial support by the Deutsche Forschungsgemeinschaft through grant SCHR 303/1-1 and through the collaborative research center SFB 813 is gratefully acknowledged.

References

1 *Ultrafast Infrared and Raman Spectroscopy*, ed. M. D. Fayer, Marcel Dekker, New York, 2001.
2 J. L. Skinner, *Theor. Chem. Acc.*, 2011, **128**, 147.
3 E. T. J. Nibbering and T. Elsaesser, *Chem. Rev.*, 2004, **104**, 1887.
4 S. Woutersen, U. Emmerichs and H. J. Bakker, *Science*, 1997, **278**, 658.
5 H.-K. Nienhuys, S. Woutersen, R. A. van Santen and H. J. Bakker, *J. Chem. Phys.*, 1999, **111**, 1494.
6 R. Laenen, C. Rauscher and A. Laubereau, *Phys. Rev. Lett.*, 1998, **80**, 2622.
7 S. Bratos, G. M. Gale, G. Gallot, F. Hache, N. Lascoux and J.-C. Leicknam, *Phys. Rev. E: Stat. Phys., Plasmas, Fluids, Relat. Interdiscip. Top.*, 2000, **61**, 5211.
8 H. J. Bakker, H.-K. Nienhuys, G. Gallot, N. Lascoux, G. M. Gale, J.-C. Leicknam and S. Bratos, *J. Chem. Phys.*, 2002, **116**, 2592.
9 C. J. Fecko, J. D. Eaves, J. J. Loparo, A. Tokmakoff and P. L. Geissler, *Science*, 2003, **301**, 1698.
10 Z. Wang, A. Pakoulev, Y. Pang and D. D. Dlott, *J. Phys. Chem. A*, 2004, **108**, 9054.

11 D. Schwarzer, J. Lindner and P. Vöhringer, *J. Chem. Phys.*, 2005, **123**, 161105.
12 D. Schwarzer, J. Lindner and P. Vöhringer, *J. Phys. Chem. A*, 2006, **110**, 2858.
13 S. Ashihara, N. Huse, A. Espagne, E. T. J. Nibbering and T. Elsaesser, *Chem. Phys. Lett.*, 2006, **424**, 66.
14 J. Lindner, P. Vöhringer, M. S. Pshenichnikov, D. Cringus, D. A. Wiersma and M. Mostovoy, *Chem. Phys. Lett.*, 2006, **421**, 329.
15 A. J. Lock and H. J. Bakker, *J. Chem. Phys.*, 2002, **117**, 1708.
16 J. Lindner, D. Cringus, M. S. Pshenichnikov and P. Vöhringer, *Chem. Phys.*, 2007, **341**, 326.
17 T. Steinel, J. B. Asbury, J. Zheng and M. D. Fayer, *J. Phys. Chem. A*, 2008, **108**, 10957.
18 D. E. Moilanen, E. E. Fenn, Y. S. Lin, J. L. Skinner, B. Bagchi and M. D. Fayer, *Proc. Natl. Acad. Sci. U. S. A.*, 2008, **105**, 5295.
19 H. J. Bakker, Y. L. A. Rezus and R. L. A. Timmer, *J. Phys. Chem. A*, 2008, **112**, 11523.
20 T. Schäfer, J. Lindner, P. Vöhringer and D. Schwarzer, *J. Chem. Phys.*, 2009, **130**, 224502.
21 T. Schäfer, D. Schwarzer, J. Lindner and P. Vöhringer, *J. Chem. Phys.*, 2008, **128**, 064502.
22 J. Lindner, A.-N. Unterreiner and P. Vöhringer, *Chem. Phys. Chem.*, 2006, **7**, 363.
23 J. Lindner, A.-N. Unterreiner and P. Vöhringer, *J. Chem. Phys.*, 2008, **129**, 064514.
24 A. J. Birch and H. Smith, *Q. Rev., Chem. Soc.*, 1958, **12**, 17.
25 *The Physics ans Physical Chemistry of Water*, ed. F. Franks, Plenum, New York, 1972.
26 M. A. Ricci, M. Nardone, F. P. Ricci, C. Andreani and A. K. Soper, *J. Chem. Phys.*, 1995, **102**, 7650.
27 H. Thompson, J. C. Wasse, N. T. Skipper, S. Hayama, D. T. Bowron and A. K. Soper, *J. Am. Chem. Soc.*, 2003, **125**, 2572.
28 A. D. Boese, A. Chandra, J. M. L. Martin and D. Marx, *J. Chem. Phys.*, 2003, **119**, 5965.
29 A. Tongraar, T. Kerdcharoen and S. Hannongbua, *J. Phys. Chem. A*, 2006, **110**, 4924.
30 D. W. Oxtoby, *Adv. Chem. Phys.*, 1981, **47**, 487.
31 R. Rey and J. T. Hynes, *J. Chem. Phys.*, 1996, **104**, 2356.
32 R. Rey, K. B. Møller and J. T. Hynes, *Chem. Rev.*, 2004, **104**, 1915.
33 C. P. Lawrence and J. L. Skinner, *J. Chem. Phys.*, 2002, **117**, 5827.
34 C. P. Lawrence and J. L. Skinner, *J. Chem. Phys.*, 2003, **119**, 1623.
35 J. K. Brown, C. B. Harris and J. C. Tully, *J. Chem. Phys.*, 1988, **89**, 6687.
36 R. M. Whitnell, K. R. Wilson and J. T. Hynes, *J. Chem. Phys.*, 1992, **96**, 5354.
37 V. S. Vikhrenko, C. Heidelbach, D. Schwarzer, V. B. Nemtsov and J. Schroeder, *J. Chem. Phys.*, 1998, **110**, 5273.
38 A. Kandratsenka, J. Schroeder, D. Schwarzer and V. S. Vikhrenko, *Phys. Chem. Chem. Phys.*, 2007, **9**, 1688.
39 A. Kandratsenka, J. Schroeder, D. Schwarzer and V. S. Vikhrenko, *J. Chem. Phys.*, 2009, **130**, 174507.
40 R. Rey, F. Ingrosso, T. Elsaesser and J. T. Hynes, *J. Phys. Chem. A*, 2009, **113**, 8949.
41 J. M. L. Martin, T. J. Lee and P. R. Taylor, *J. Chem. Phys.*, 1992, **97**, 8361.
42 M. Snels, H. Hollenstein and M. Quack, *J. Chem. Phys.*, 2006, **125**, 194319.
43 E. B. Wilson Jr., J. C. Decius and P. C. Cross, *Molecular Vibrations*, McGraw-Hill Book Company Inc., New York, 1955.
44 L. D. Landau and E. M. Lifshitz, *Quantum Mechanics: Non-relativistic Theory. Course of Theoretical Physics*, vol. 3, Pergamon Press, Oxford, 1991.
45 M. Diraison, G. J. Martyna and M. E. Tuckerman, *J. Chem. Phys.*, 1999, **111**, 1096.
46 T. Kristóf, J. Vorholz, J. Liszi, B. Rumpf and G. Maurer, *Mol. Phys.*, 1999, **97**, 1129.
47 K. Refson, *Comput. Phys. Commun.*, 2000, **126**, 310.
48 M. P. Allen and D. J. Tildesley, *Computer Simulation of Liquids*, Clarendon Press, Oxford, 1989.
49 W. H. Press, S. H. Teukolsky, W. T. Vetterling and B. P. Flannery, *Numerical Recipes*, Cambridge University Press, Cambridge, 2007.
50 C. P. Lawrence and J. L. Skinner, *J. Chem. Phys.*, 2003, **119**, 3840.
51 M. Snels, H. Hollenstein and M. Quack, *J. Chem. Phys.*, 2003, **119**, 7893.
52 A. Bromberg, S. Kimel and A. Ron, *Chem. Phys. Lett.*, 1977, **46**, 262.
53 S. A. Egorov, K. F. Everitt and J. L. Skinner, *J. Phys. Chem. A*, 1999, **103**, 9494.
54 J. L. Skinner and K. Park, *J. Phys. Chem. B*, 2001, **105**, 6716.

